# Early self-assembled stages in epitaxial $SrRuO_3$ on $LaAlO_3$

E. Vasco,[a] R. Dittmann, S. Karthäuser, and R. Waser
*Institut für Festkörperforschung, Forschungszentrum Jülich, D-52425 Jülich, Germany*

(Received 28 October 2002; accepted 12 February 2003)

The stress-induced self-assembled growth of $SrRuO_3$ on $LaAlO_3$ was studied by atomic force microscopy and x-ray diffraction. $SrRuO_3$ epitaxially grown on $LaAlO_3$ by pulsed laser deposition shows two types of out-of-plane arrangements and four in-plane matches. The lattice mismatch (stress) produced by these arrangements was estimated and correlated with the $SrRuO_3$ growth dynamics. After 1 nm, the $SrRuO_3$ film surface exhibits a ripple structure, which serves as a template for the development of a nanopattern of flat islands. These islands coalesce anisotropically resulting in a regular array of ''infinite'' wires. The wire coalescence for the 12–20 nm thick film nullifies the surface symmetry, while $SrRuO_3$ keeps growing in three dimensions. © *2003 American Institute of Physics.* [DOI: 10.1063/1.1566798]

For decades, self-organized semiconductor nanostructures have attracted extensive technological and scientific interest.[1] Motivated by the search for novel electrical, magnetic, optical and ferroelectric properties based on the confinement effect, this interest has spread to other emerging fields such as metal- and oxide-based nanotechnology. In this context, special attention has been paid to the synthesis of nanostructures. An attractive fabrication route is provided by the ''self-assembled'' deposition techniques which take advantage of the highly corrugated surface reconstructions,[2] periodic arrangement of kinks[3] as well as of the stress-induced surface modulations[4,5] to create the patterned nanostructure. So far, the physical mechanisms that drive self-organizing growth have been studied in great detail in semiconductors,[1] less frequently in metallic systems,[3,4] and rarely in epitaxial oxides as grown from vapor deposition techniques,[6] despite the increasing technological interest focused on these latter materials (note, for instance, the crucial advances in high-$T_c$ superconductors, ferroelectrics and colossal magnetoresistors[7]). The tendency of some oxides toward self-organized growth, forming regular arrays of three-dimensional (3D) uniform structures, offers enormous potential for the implementation of new nanodevices, while at the same time constitutes a real scientific challenge.

$SrRuO_3$ (SRO) is a magnetic oxide of increasing interest for its structural and chemical similarity with $LaMnO_3$-based colossal magnetoresistive materials. It has a $GdFeO_3$-type orthorhombic structure (space group $Pnma$) with lattice parameters $a=5.567$ Å, $b=5.535$ Å and $c=7.845$ Å, which can be described as a slightly distorted pseudocubic perovskite cell ($a_c=3.93$ Å, $\alpha=\beta=90°$ and $\gamma=89.67°$). At temperatures lower than $T_c=160$ K,[8] SRO is a ferromagnetic oxide with anisotropic magnetotransport properties that are related to its crystalline order. Similar to magnetoresistive materials, epitaxial SRO shows a decrease in resistivity as the magnetic order improves.[9] Since this oxide is a potential candidate for magnetic and magnetoresistive memories, the task of producing a SRO-based high-density device constitutes a technological challenge. SRO has been epitaxially grown by pulsed laser deposition and sputtering on several substrates: $SrTiO_3$,[10,11] $LaAlO_3$,[12–14] STO/$LaAlO_3$ and buffered Si.[15] $SrRuO_3$ grows on a singular (100)$LaAlO_3$ (LAO) surface in 3D growth mode, and exhibits two possible out-of-plane orientations: [110]SRO//[001]LAO (Refs. 13 and 14) or 45°-rotated cube-on-cube [001]SRO//[001]LAO,[12,14] as shown below. LAO has a rhombohedral structure ($a=5.357$ Å and $\alpha=60.1°$) that can be simplified in terms of a pseudocubic unit cell with lattice parameter $a_c=3.79$ Å. In this work, the crystallographic indices of SRO and LAO are referred to their orthorhombic and pseudocubic unit cells, respectively.

The SRO films were pulsed laser deposited on (100)LAO using a KrF excimer laser with 16 ns pulses (5 J/cm$^2$ and 10 Hz) at 248 nm. The deposition was made in a high vacuum chamber (base pressure: $1\times10^{-5}$ mbar), in the presence of oxygen dynamic pressure of 0.5 mbar at 700 °C. The films grew at a rate of 0.18 Å/pulse. The morphology was characterized by atomic force microscopy (AFM) using equipment manufactured by Surface Imaging System in non-contact mode. A Si cantilever with a nominal radius of 10 nm and a spring constant of $k=40$ N/m, was used. $\theta$–$2\theta$ and $\phi$-scan x-ray measurements were performed in a X'Pert Philips diffractometer using Cu $K\alpha$ radiation. The film thickness was determined from the x-ray interference fringes in a low angle $\theta$–$2\theta$ scan, and checked by transmission electron microscopy.

Figure 1 shows the steps in the morphologic evolution of the SRO film. The surface symmetries provided by their height–height correlation maps were included in the corresponding insets. The surface of the 1 nm (two or three unit cells) thick film [Fig. 1(b)] grown on flat LAO [Fig. 1(a)] shows a periodic ripple structure, which is a result of the relief of stress that appears in the coherent SRO/LAO interface[14] due to the high lattice mismatch (~3%–4%) between the two materials. In the absence of plastic relaxation at these thicknesses,[14] the film releases stress via the creation of additional surface roughness. In fact, the surface of an elastically strained film is unstable with respect to growth, and generates perturbations with wavelength larger than a certain crossover: $\xi_\perp=\pi\varphi M/\sigma^2$,[16] $\varphi$ being the interface ten-

[a]Author to whom correspondence should be addressed; electronic mail: e.vasco.matias@fz-juelich.de

 

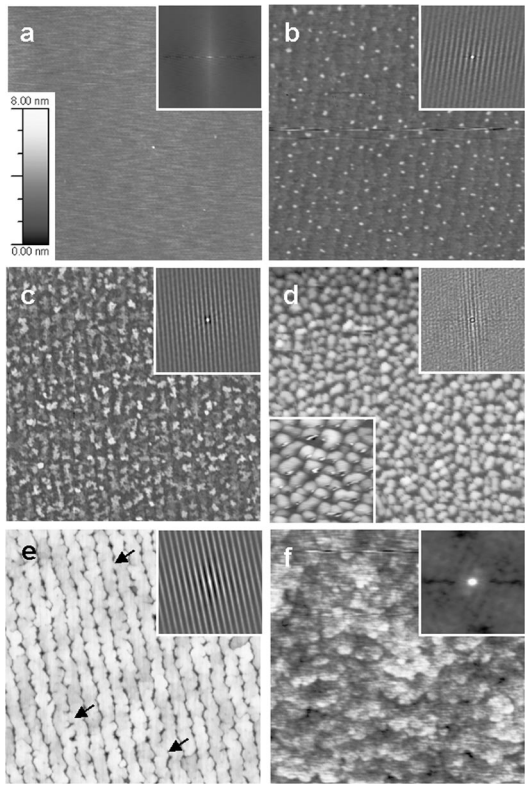


FIG. 1. Evolution of the surface morphology of SRO with the film thickness: 0 nm or LAO (001) surface (a), and 1 (b), 2.5 (c), 5 (d), 12 (e) and 20 nm (f). The upper insets show the corresponding height–height correlation maps. The lower inset in (d) displays details for $1\times1$ $\mu m^2$. The area scanned by AFM was $5\times5$ $\mu m^2$. Areas of early wire coalescence are pointed out in (e). The height scale for all pictures are shown in (a).

sion; $M$ the elastic SRO modulus; and $\sigma$ the average stress. Additional nucleation centers form on the rippled surface [Fig. 1(b)], clear evidence of the fact that the ripples confine the nucleation area, and prevent the formation of centers in the interripple regions. The ripple structure produces a nonuniform distribution of stress at the film surface. Thus the interripple areas remain stressed and unfavorable to nucleation. 3D irregular islands are developed from these nucleation centers in the 2.5 nm thick film [Fig. 1(c)]. The islands are arranged in unconnected rows while remaining laterally confined, and form a nanoassembled pattern. The islands coarsen into more regular form and uniform size as the film thickness increases [Fig. 1(d)]. The inset in Fig. 1(d) demonstrates that the row symmetry of the growth surface is preserved even when a more disordered surface structure emerges. Anisotropic grain coalescence in the nonconfined direction produces a compact regular array of wires separated by abrupt boundaries [Fig. 1(e)]. This anisotropy is likely connected to the fact that surface stress relaxation partially hinders the diffusion of mobile species between ripples through an increase of the hopping barrier in this direction. Early evidence of wire coalescence is shown in Fig. 1(e). Finally, as a result of this coalescence, the surface row symmetry disappears at thicknesses higher than 20 nm [Fig. 1(f)].

Figure 2 shows typical height profiles in two high symmetry directions of the growth surface. The patterned islands exhibit flat tops separated by abrupt steps. The step heights correspond to the number of unit-cell parameters in orthorhombic [110] directions (~3.92 Å), suggesting that growth proceeds unit cell by unit cell. This is in agreement with the SrO-terminated SRO model proposed by Choi *et al.*,[11] based on the high volatility of Ru atoms.

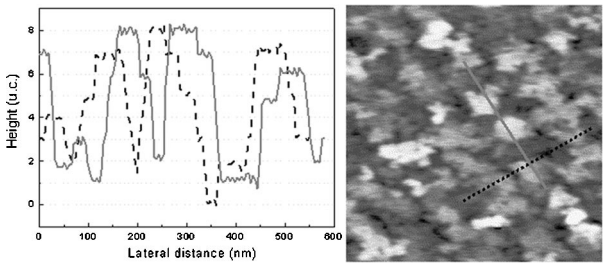


FIG. 2. Height profiles in two directions of high symmetry of the surface of the 2.5 nm thick SRO film.

The root mean square roughness, $w$, of the sample surfaces $[h(r)]$ was calculated from $10\times10$ $\mu m^2$ AFM images. The ripple period, $\xi_\perp$, and grain size in the ripple axis direction, $\xi_\parallel$, were estimated from an average of the points of interest ($\chi_1$ and $\chi_2$) of one-dimensional (1D) height–height correlation functions, $hhc(x)=\langle[h(r+x)-(h)][h(r)-(h)]\rangle$. $\chi_1$ and $\chi_2$ are defined as $hhc(\chi_1)=0$ and $hhc(\chi_2/2)=hhc(0)/2$, respectively. The data were scaled with respect to the film thickness, $d$, (i.e., $w\sim d^\beta$, $\xi_\perp$ and $\xi_\parallel\sim d^p$; with $\beta$ and $p$ the growth and coarsening coefficient, respectively) in order to determine the mechanisms that operate during film growth according to the dynamic scaling theory.[17] The data obtained as well as the best fits are shown in Fig. 3. The roughness and the average grain size increase monotonously at a log–log rate of $\beta=p_\parallel=0.75$ as $d$ increases up to film thicknesses of around 10 nm. This implies that the 3D grains maintain their form (height/diameter ratio ≈const) during coarsening, and suggests that growth is controlled by instabilities that hinder surface relaxation, thereby

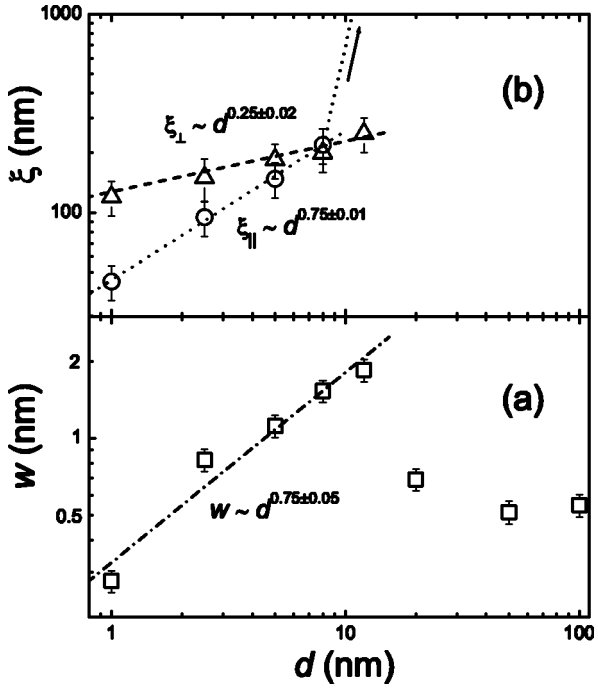


FIG. 3. Evolution of surface roughness (a), the ripple period and the grain average (b) with the SRO film thickness. The straight lines correspond to fitted scaling expressions whose coefficients are shown.

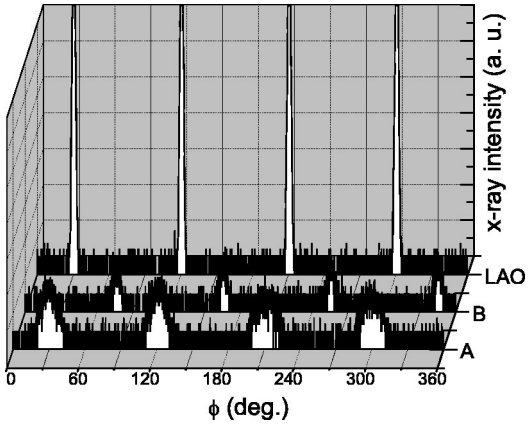


FIG. 4. $\phi$-scan spectra of the 12 nm thick film of LAO 103 diffraction (spectrum LAO); SRO 221 diffraction, assuming arrangement type A (a) and SRO 206 diffraction, assuming arrangement type B (b).

inhibiting lateral redistribution of incident particles ($\beta > 0.5$).[17] These perturbations can be ascribed to the influence of stress on the film growth dynamics, as seen in Fig. 1. The slow increase ($p_{\perp} = 0.25$) of the ripple period reveals progressive stress relaxation with an increase in film thickness (see the equation above), which is a result of two-dimensional (2D) to 3D Stranski–Krastanov growth mode. Since the ripple structure laterally confines grain coarsening, once $\xi_{\parallel} \approx \xi_{\perp}$, the grain form is lost and the grains tend to grow mainly along the ripple's axis. This preferential growth gives rise to the anisotropic coalescence process, which creates the array of ''infinite'' wires. After wire coalescence, the roughness decreases abruptly and remains constant ($w \approx 0.5$ nm).

In order to investigate the origin of the anisotropy in SRO growth mode, studies of the epitaxial arrangement between the nanoassembled SRO film and the LAO (001) surface by $\theta$–$2\theta$ and $\phi$-scan x-ray measurements were performed. The $\theta$–$2\theta$ spectra (not presented here) show only the SRO 110/001 peak ($2\theta = 22.6°$), harmonics, and characteristic diffractions of the substrate. The $\phi$-scan spectra (Fig. 4), however, revealed the existence of at least two epitaxial arrangements, each one formed by two in-plane matches: SRO⟨110⟩//LAO⟨001⟩ (arrangement type A) with SRO[001]//LAO[100] and SRO[001]//LAO[010]; and SRO⟨001⟩//LAO⟨001⟩ (arrangement type B) with SRO[100]//LAO[110] and SRO[100]//LAO[−110]. The lattice mismatch, $m$, of each arrangement was estimated from the lattice parameters obtained by deconvoluting the SRO 110/001 peak into two pseudo-Voight contributions and the $2\theta$ positions of the SRO 221 and SRO 206 diffractions. Thus, for arrangement A: $m_{//\mathrm{SRO}[001]} \approx -3.5\%$ and $m_{//\mathrm{SRO}[-110]} \approx -3.6\%$; for the arrangement B: $m_{//\mathrm{SRO}[100]} \approx -3.9\%$ and $m_{//\mathrm{SRO}[010]} \approx -3.3\%$. Note that although both arrangements result in significant biaxial compression of the SRO film, the degree of anisotropy produced by arrangement B is meaningfully higher. As a consequence, we suggest the presence of arrangement B is related to the origin of surface row symmetry.

Preliminary studies demonstrate that nanopatterned films keep characteristic functional properties (i.e., metallic conductivity and ferromagnetic nature) of the compact SRO films. The resistivity, $\rho$, of row-patterned SRO increased with the temperature from $\rho(T = 40\ \mathrm{K}) \approx 86\ \mu\Omega$-cm up to $\rho(T = 273\ \mathrm{K}) \approx 279\ \mu\Omega$-cm. The Curie temperature ($T_C \approx 155$ K) was slightly lower than that of bulk SRO, which is likely due to stress in the system.[18]

In conclusion, nanopatterned epitaxial SRO was successfully prepared on LAO by pulsed laser deposition. The compressive biaxial stress originating in the coherent SRO/LAO interface induces a ripple structure in the SRO growth surface. The ripple structure plays a crucial role in the development of nanoarrays of islands and wires. Scaling and x-ray analysis suggested that the stress anisotropically destabilizes the growth surface and results in Stranski–Krastanov growth mode.

The authors thank S. Stein for the preliminary functional results and Dr. A Teren for help with the manuscript. This work was supported by the Deutsche Bundesministerium für Bildung und Forschung under Grant No. 13N8361.

[1] J. A. Floro, E. Chanson, M. B. Sinclair, L. B. Freud, and G. A. Lucadamo, Appl. Phys. Lett. **73**, 951 (1998); J. A. Floro, G. A. Lucadamo, E. Chanson, L. B. Freud, M. B. Sinclair, R. D. Twesten, and R. Q. Hwang, Phys. Rev. Lett. **80**, 4717 (1998).
[2] Y. P. Zhang, L. Yan, S. S. Xie, S. J. Pang, and H.-J. Gao, Appl. Phys. Lett. **79**, 3317 (2001).
[3] B. Voigtländer, G. Meyer, and N. M. Amer, Phys. Rev. B **44**, 10 354 (1991); O. Fruchart, M. Klaua, J. Barthel, and J. Kirschner, Phys. Rev. Lett. **83**, 2769 (1999).
[4] H. Brune, M. Giovannini, K. Bromann, and K. Kern, Nature (London) **394**, 451 (1998).
[5] O. G. Schmidt, N. Y. Jin-Phillipp, C. Lange, U. Denker, K. Eberl, R. Schreiner, H. Gräbeldinger, and H. Schweizer, Appl. Phys. Lett. **77**, 4139 (2000).
[6] M. Alexe, J. F. Scott, C. Curran, N. D. Zakharov, D. Hesse, and A. Pignolet, Appl. Phys. Lett. **73**, 1592 (1998); J. C. Jiang, E. I. Meletis, and K. I. Gnanasekar, *ibid.* **80**, 4831 (2002).
[7] D. Dijkkamp, T. Venkatesan, X. D. Xu, S. A. Shaheen, N. Jisrawi, Y. H. Min-Lee, W. L. McCean, and M. Croft, Appl. Phys. Lett. **51**, 619 (1987); J. S. Horwitz, K. S. Grabowski, D. B. Chrisey, and R. E. Leuchtner, *ibid.* **59**, 1565 (1991); R. Von Helmolt, J. Wecker, B. Holzapfel, L. Schultz, and K. Samwer, Phys. Rev. Lett. **71**, 2331 (1994).
[8] A. Callaghan, C. W. Moeller, and R. Ward, Inorg. Chem. **5**, 1572 (1966).
[9] D. B. Kacedom, R. A. Rao, and C. B. Eom, Appl. Phys. Lett. **71**, 1724 (1997).
[10] J. C. Jiang, W. Tian, X. Q. Pan, Q. Gan, and C. B. Eom, Appl. Phys. Lett. **72**, 2963 (1998).
[11] J. Choi, C. B. Eom, G. Rijnders, H. Rogalla, and D. H. A. Blank, Appl. Phys. Lett. **79**, 1447 (2001).
[12] X. D. Wu, S. R. Foltyn, R. C. Dye, Y. Coulter, and R. E. Muenchausen, Appl. Phys. Lett. **62**, 2434 (1993).
[13] R. A. Rao, Q. Gan, and C. B. Eom, Appl. Phys. Lett. **71**, 1171 (1997).
[14] J. C. Jiang and X. Q. Pan, J. Appl. Phys. **89**, 6365 (2001).
[15] J. Roldán, F. Sánchez, V. Trtik, C. Guerrero, F. Benitez, C. Ferrater, and M. Varela, Appl. Surf. Sci. **154**, 159 (2000).
[16] D. J. Srolovitz, Acta Metall. **37**, 621 (1989); L. E. Shilkrot, D. J. Srolovitz, and J. Tersoff, Appl. Phys. Lett. **77**, 304 (2000).
[17] A. L. Barabási and H. E. Stanley, *Fractal Concepts in Surface Growth* (Cambridge University Press, New York, 1995).
[18] Q. Gan, R. A. Rao, C. B. Eom, J. L. Garrett, and M. Lee, Appl. Phys. Lett. **72**, 978 (1998).